# Detection and monitoring of the multiple inflammatory responses by photoacoustic molecular imaging using selectively targeted gold nanorods

**Seunghan Ha,[1] Andrew Carson,[1] Ashish Agarwal,[2] Nicholas A. Kotov,[2] and Kang Kim[1,3,*]**

[1]*Center for Ultrasound Molecular Imaging and Therapeutics, University of Pittsburgh and University of Pittsburgh Medical Center, Pittsburgh, PA, 15261, USA*
[2]*Department of Chemical Engineering, University of Michigan, Ann Arbor, MI, 48109-2125, USA*
[3]*Department of Bioengineering, University of Pittsburgh, PA, 15261, USA*
**kangkim@upmc.edu*

**Abstract:** *In vitro* cell experiments have been performed to detect and monitor the upregulation of intercellular adhesion molecule-1 (ICAM-1) and E-selectin simultaneously by photoacoustic molecular imaging (PMI). Human umbilical vein endothelial cells (HUVECs) were grown on gelatin-coated glass slides and stimulated with inflammatory cytokines to induce the expression of the inflammatory biomarkers, ICAM-1 and E-selectin. Gold nanorods (GNRs) of aspect ratio (AR) 1:3 with absorption centered at 715 nm conjugated to anti-ICAM-1 antibody and GNRs of AR 1:3.5 with absorption centered at 800 nm conjugated to anti-E-selectin were exposed to HUVECs with different stimulation conditions. A focused high frequency ultrasonic transducer (60 MHz, f/1.5) was used to scan the photoacoustic (PA) signal over the top surface of the cell containing slides. Averaged PA signal intensity from the stimulated cells was about 3 folds higher (~10 dB) compared to the un-stimulated cells for both ICAM-1 and E-selectin. The strong binding of GNRs to the stimulated HUVEC cells was evidenced by fluorescence imaging. Exposure of HUVEC cells to GNRs conjugated to isotype control antibodies confirms a low level non-specific binding. Also, at 0, 2, 6, and 24 hours after inflammatory stimulation, the HUVECs were exposed to GNRs conjugated anti-ICAM-1 antibody and anti-E-selectin antibody. PA intensity at each stage of inflammation compares well with fluorescence imaging and rt-PCR quantification.



**OCIS codes:** (000.0000) General; (000.2700) General science.

## References and links

1. G. K. Hansson, "Inflammation, atherosclerosis, and coronary artery disease," N. Engl. J. Med. **352**(16), 1685–1695 (2005).
2. P. T. Kovanen, M. Kaartinen, and T. Paavonen, "Infiltrates of activated mast cells at the site of coronary atheromatous erosion or rupture in myocardial infarction," Circulation **92**(5), 1084–1088 (1995).
3. S. Verma and T. J. Anderson, "Fundamentals of endothelial function for the clinical cardiologist," Circulation **105**(5), 546–549 (2002).
4. S. Verma, M. R. Buchanan, and T. J. Anderson, "Endothelial function testing as a biomarker of vascular disease," Circulation **108**(17), 2054–2059 (2003).
5. M. Mitka, "Biomarkers for coronary heart disease: predictive value or background noise?" JAMA **292**(23), 2824–2825 (2004).
6. P. Libby, P. M. Ridker, and A. Maseri, "Inflammation and atherosclerosis," Circulation **105**(9), 1135–1143 (2002).
7. R. G. Collins, R. Velji, N. V. Guevara, M. J. Hicks, L. Chan, and A. L. Beaudet, "P-Selectin or intercellular adhesion molecule (ICAM)-1 deficiency substantially protects against atherosclerosis in apolipoprotein E-deficient mice," J. Exp. Med. **191**(1), 189–194 (2000).

#141286 - $15.00 USD Received 18 Jan 2011; revised 16 Feb 2011; accepted 17 Feb 2011; published 23 Feb 2011

8. C. Kim, E. C. Cho, J. Chen, K. H. Song, L. Au, C. Favazza, Q. Zhang, C. M. Cobley, F. Gao, Y. Xia, and L. V. Wang, "*In vivo* molecular photoacoustic tomography of melanomas targeted by bioconjugated gold nanocages," ACS Nano **4**(8), 4559–4564 (2010).
9. A. De La Zerda, C. Zavaleta, S. Keren, S. Vaithilingam, S. Bodapati, Z. Liu, J. Levi, B. R. Smith, T.-J. Ma, O. Oralkan, Z. Cheng, X. Chen, H. Dai, B. T. Khuri-Yakub, and S. S. Gambhir, "Carbon nanotubes as photoacoustic molecular imaging agents in living mice," Nat. Nanotechnol. **3**(9), 557–562 (2008).
10. D. Pan, M. Pramanik, A. Senpan, J. S. Allen, H. Zhang, S. A. Wickline, L. V. Wang, and G. M. Lanza, "Molecular photoacoustic imaging of angiogenesis with integrin-targeted gold nanobeacons," FASEB J. fj.10-171728 (2010).
11. A. Agarwal, S. W. Huang, M. O'Donnell, K. C. Day, M. Day, N. A. Kotov, and S. Ashkenazi, "Targeted gold nanorod contrast agent for prostate cancer detection by photoacoustic imaging," Appl. Phys. Lett. **102**(6), 064701 (2007).
12. S. Sethuraman, J. H. Amirian, S. H. Litovsky, R. W. Smalling, and S. Y. Emelianov, "Spectroscopic intravascular photoacoustic imaging to differentiate atherosclerotic plaques," Opt. Express **16**(5), 3362–3367 (2008).
13. A. Conjusteau, S. A. Ermilov, D. Lapotko, H. Liao, J. Hafner, M. Eghtedari, M. Motamedi, N. A. Kotov, and A. A. Oraevsky, "Metallic nanoparticles as optoacoustic contrast agents for medical imaging," Proc. SPIE **6086**, 60860K, 60860K-9 (2006).
14. P. C. Li, C. W. Wei, C. K. Liao, C. D. Chen, K. C. Pao, C. R. C. Wang, Y. N. Wu, and D. B. Shieh, "Photoacoustic imaging of multiple targets using gold nanorods," IEEE Trans. Ultrason. Ferroelectr. Freq. Control **54**(8), 1642–1647 (2007).
15. L. M. Liz-Marzán, "Tailoring surface plasmons through the morphology and assembly of metal nanoparticles," Langmuir **22**(1), 32–41 (2006).
16. J. A. Copland, M. Eghtedari, V. L. Popov, N. A. Kotov, N. Mamedova, M. Motamedi, and A. A. Oraevsky, "Bioconjugated gold nanoparticles as a molecular based contrast agent: implications for imaging of deep tumors using optoacoustic tomography," Mol. Imaging Biol. **6**(5), 341–349 (2004).
17. K. Kim, S. W. Huang, S. Ashkenazi, M. O'Donnell, A. Agarwal, N. A. Kotov, M. F. Denny, and M. J. Kaplan, "Photoacoustic imaging of early inflammatory response using gold nanorods," Appl. Phys. Lett. **90**(22), 223901 (2007).
18. K. Kim, A. Agarwal, A. M. Mcdonald, R. M. Moore, and D. D. Myers, Jr, R.S. Witte, S.W. Huang, S. Ashkenazi, M.J. Kaplan, T.W. Wakefield, M. O'Donnell, and N.A. Kotov, "*In vivo* imaging of inflammatory responses by photoacoustic using cell-targeted gold nanorods (GNRs) as contrast agent," Proc. SPIE **6856**, 68560H.1–68560.H8 (2008).
19. E. M. Shevach, *Current Protocols in Immunology* (Wiley, New York, 2002), Chap. 5.
20. J. Doukas, and J. S. Pober, "IFN-gamma enhances endothelial activation induced by tumor necrosis factor but not IL-1," J. Immunol. **145**(6), 1727–1733 (1990).
21. B. Nikoobakht, and M. A. El-Sayed, "Preparation and Growth Mechanism of Gold Nanorods (NRs) Using Seed-Mediated Growth Method," Chem. Mater. **15**(10), 1957–1962 (2003).
22. C. J. Murphy and N. R. Jana, "Controlling the aspect ratio of inorganic nanorods and nanowires," Adv. Mater. (Deerfield Beach Fla.) **14**(1), 80–82 (2002).
23. A. Gole and C. J. Murphy, "Biotin-streptavidin-induced aggregation of gold nanorods: tuning rod-rod orientation," Langmuir **21**(23), 10756–10762 (2005).
24. Y. Wang, Z. Tang, S. Tan, and N. A. Kotov, "Biological assembly of nanocircuit prototypes from protein-modified CdTe nanowires," Nano Lett. **5**(2), 243–248 (2005).
25. J. Lee, A. O. Govorov, J. Dulka, and N. A. Kotov, "Bioconjugates of CdTe nanowires and Au Nanoparticles: plasmon-exciton interactions, luminescence enhancement, and collective effects," Nano Lett. **4**(12), 2323–2330 (2004).
26. S. Wang, N. Mamedova, N. A. Kotov, W. Chen, and J. Studer, "Antigen/antibody immunocomplex from CdTe nanoparticle bioconjugates," Nano Lett. **2**(8), 817–822 (2002).
27. N. N. Mamedova, N. A. Kotov, A. L. Rogach, and J. Studer, "Albumin-CdTe nanoparticle bioconjugates: preparation, structure, and interunit energy transfer with antenna effect," Nano Lett. **1**(6), 281–286 (2001).
28. S.H. Ha, J.S. Kim, S. Tripathy, A. Carson, M. Grata, A. Agarwal, N.A. Kotov, F.S. Villanueva, and K. Kim, "Simultaneous photoacoustic detection of multiple inflammatory biomarkers using bioconjugated gold nanorods as selective targeting agents," presented at 2010 IEEE International Ultrasonics Symposium (IUS), San Diego, California, USA, Oct. 11–14, 2010.
29. K. Karmann, W. Min, W. C. Fanslow, and J. S. Pober, "Activation and homologous desensitization of human endothelial cells by CD40 ligand, tumor necrosis factor, and interleukin 1," J. Exp. Med. **184**(1), 173–182 (1996).
30. A. Rahman, J. Kefer, M. Bando, W. D. Niles, and A. B. Malik, "E-selectin expression in human endothelial cells by TNF-alpha-induced oxidant generation and NF-kappaB activation," Am. J. Physiol. **275**(3 Pt 1), L533–L544 (1998).
31. H. F. Zhang, K. Maslov, G. Stoica, and L. V. Wang, "Functional photoacoustic microscopy for high-resolution and noninvasive *in vivo* imaging," Nat. Biotechnol. **24**(7), 848–851 (2006).
32. Y. Wang, K. Maslov, C. Kim, S. Hu, and L. V. Wang, "Integrated photoacoustic and fluorescence confocal microscopy," IEEE Trans. Biomed. Eng. **57**(10), 2576–2578 (2010).
33. E. E. Connor, J. Mwamuka, A. Gole, C. J. Murphy, and M. D. Wyatt, "Gold nanoparticles are taken up by human cells but do not cause acute cytotoxicity," Small **1**(3), 325–327 (2005).

#141286 - $15.00 USD Received 18 Jan 2011; revised 16 Feb 2011; accepted 17 Feb 2011; published 23 Feb 2011

34. S. Mallidi, T. Larson, J. Tam, P. P. Joshi, A. Karpiouk, K. Sokolov, and S. Emelianov, "Multiwavelength photoacoustic imaging and plasmon resonance coupling of gold nanoparticles for selective detection of cancer," Nano Lett. **9**(8), 2825–2831 (2009).
35. B. Wang, J. L. Su, A. B. Karpiouk, K. V. Sokolov, R. W. Smalling, and S. Y. Emelianov, "Intravascular photoacoustic imaging," IEEE J. Sel. Top. Quantum Electron. **16**(3), 588–599 (2010).

## 1. Introduction

Recent reports have shown that inflammation plays a key role in a variety of systemic diseases such as atherosclerosis, coronary artery disease (CAD), rheumatoid arthritis (RA), and systemic lupus erythematosus [1]. In the vascular inflammation response, immune cells dominate early atherosclerotic lesions, where they activate inflammation, leading to progression of the lesions and acute coronary syndromes [1]. Activated immune cells produce inflammation primarily through the production of proinflammatory cytokines [2]. This widespread, complex, and multifactorial nature of vascular disease has led cardiovascular researchers and clinicians to investigate new strategies for prediction, prevention, and treatment [1]. Additionally, endothelial cell dysfunction can also contribute to vascular disease by contributing to vasoconstriction, leukocyte adherence, platelet activation, mitogenesis, oxidation, thrombosis, impaired coagulation, vascular inflammation, and atherosclerosis [3]. Understanding these endothelial cell responses has led to the development of diagnostics and therapeutics technology [4].

Inflammatory biomarkers may predate clinical disease [5,6]. The importance of the inflammatory response in atherosclerosis is indicated by the increased expression of adhesion molecules, pro-inflammatory cytokines, and growth factors in lesions and lesion-prone areas and by increased resistance to vascular disease in knock-out mice lacking certain cytokines [7]. Prospective epidemiological studies have suggested that vascular risk is affected by increased basal levels of inflammatory cytokines such as interleukin-6 (IL-6) and tumor necrosis factor alpha (TNF-α); cell adhesion molecules such as soluble or membrane-bound ICAM-1, E-selectin, and P-selectin; and acute-phase reactants such as C-reactive protein and fibrinogen [6]. Detection of these specific biomarkers, especially simultaneously, could show the bioactivities of inflammation and may provide prognostic information and further characterize systemic diseases such as atherosclerosis. Furthermore, the longitudinal monitoring of these transcriptional regulations may lead to a better understanding of molecular and cellular processes of diseases.

It has been shown that photoacoustic molecular imaging (PMI) using nanoparticles as targeting agents such as gold nanocages [8], carbon nanotubes [9], gold nano beacons [10], and gold nanorods (GNRs) [11–16] can be of value for detection of specific biomarkers of interest *in vitro* and *in vivo*. In our pervious PMI study, single targeting of vascular inflammation biomarker such as ICAM-1 using bio-conjugated GNRs of a fixed aspect ratio as targeting agent was demonstrated through *in vitro* HUVECs cell study and *in vivo* mouse study [17,18].

In this study, GNRs of different aspect ratios with optical absorption centered at different wavelengths were used to demonstrate simultaneous detection and time course monitoring of markers of endothelial inflammation. GNRs were selected for their unique and distinct primary absorption peaks at different wavelength depending on their aspect ratio, which makes GNRs ideal for multi-target detection. Adhesion molecules, ICAM-1 and E-selectin, were chosen as typical biomarker of inflammation and activation of endothelial cells (ECs).

## 2. Materials and methods

### *2.1. Cell preparations and immunfluorescence analysis*

Human umbilical vein endothelial cells (HUVECs) were maintained on tissue culture plates (750ml, BD, Franklin Lakes, NJ, USA) in MCDB131 media (Gibco®, Invitrogen, Carlsbad, CA, USA) supplemented with microvascular EC growth factors (EGM, Cambrex, East Rutherford, NJ, USA). Cells were then split into 12 wells of quadriPERM® ($3 \times 10^4$ cells/well, 8 mm, Sigma-Aldrich, St. Louis, MO, USA) on the surface gelatin-coated slide (Labscientific,

#141286 - $15.00 USD Received 18 Jan 2011; revised 16 Feb 2011; accepted 17 Feb 2011; published 23 Feb 2011

Inc., Livingston, NJ, USA) two days prior to experiments. Media were changed 24 hours after splitting and the cells were left un-stimulated or stimulated with the proinflammatory cytokines Interferon-gamma (IFN-γ) (Peprotech, Rocky Hill, NJ, USA) (200 ng/ml) and TNF-alpha (TNF-α) (Peprotech, Rocky Hill, NJ, USA) (25 ng/ml) for 0, 2, 6 and 24 hours. Cells were blocked for 30 min at 4 °C in blocking media (PBS; containing 1% bovine serum albumin (BSA) 1% horse serum (HS)). After removing the blocking solution, the cells were incubated for 14 hours at 4 °C with gold nanorod-conjugated FITC labeled anti-ICAM-1 (ebioscience, San Diego, CA, USA) and gold nanorod-conjugated Phycoerythrin (PE) labeled anti-E-selectin (ebioscience, San Diego, CA, USA) or isotype control antibody (Biolegend, San Diego, CA, USA). Microscope images were subsequently obtained followed by PA imaging. For bright field and the fluorescence microscopy measurements, the cells were washed 2 times (each time for 5) with PBS. The cells were then fixed in 4% paraformaldehye for 4 hours. The fluorescence microscopy was performed using an inverted microscope (X81, Olympus, Center Valley, PA, USA) and images were acquired using a CCD camera (DP71, Olympus, Center Valley, PA, USA). All images were acquired and processed using identical settings [16,19,20]. The EC expression of ICAM-1 and E-selectin was visualized by fluorescence imaging.

*2.2. Real-time quantitative PCR*

Real-time PCR (rt-PCR) was performed to quantify expression of ICAM-1 and E-selectin. Briefly, HUVEC cells were homogenized and RNA was extracted using Trizol reagent (Invitrogen, Carlsbad, CA, USA) as per manufacturer's instructions and quantified on a spectrophotometer (SmartSpec Plus, Bio-Rad, Hercules, CA, USA). mRNA was reverse transcribed using Taqman Reverse Transcriptase Reagents (Applied Biosystems, Branchburg, NJ, USA) as per manufactures instructions. Real-time PCR was performed on a ABI Prism 7000 sequence detection system (Applied Biosystems, Foster City, CA, USA) using the Absolute Blue SYBR Green kit (Thermo Fischer Scientific, Epsom, Surrey, UK). ICAM-1 and E-selectin expression in all samples was calculated by the ΔCt method as fold over Glyceraldehyde-3-phosphated dehydrogenase (GAPDH) expression as an internal control. ICAM-1 and E-selectin from un-stimulated cells was used as a reference point and fold induction of ICAM-1 and E-selectin was determined by dividing the stimulated levels by the baseline level.

*2.3. GNRs synthesize and bio-conjugation*

GNRs of aspect ratio (AR) of 1:3 or 1:3.5 were synthesized [21,22]. Their optical absorption was centered at 715 nm and 800 nm, respectively, as shown in Fig. 1. As shown, the distinct separation in the optical absorption spectrum between GNRs with different ARs enables the multiple targeting on the same site with an insignificant overlap between two different wavelengths. Synthesized GNRs have a bilayer of surfactant hexadecyltrimethylammonium bromide (CTAB) on their surface acting as a stabilizer to prevent aggregation. After removing excess CTAB, the GNRs form a pellet at the bottom of the tube, which was redispersed in de-ionized (DI) water. A layer of polyacrylic acid (PAA) (Sigma-Aldrich, St. Louis, MO, USA) was absorbed on the surface of GNRs by adding 100 µl of 10 mg/ml PAA solution to 1 ml of GNRs solution. Excess PAA in solution was removed. The layer of PAA provides the -COOH functional group required for conjugation. PAA-coated GNRs were dispersed in 10 ml of DI water followed by the addition of 1.25 ml of 1M N-ethyl-N-3-dimethylaminopropyl-carbodiimide (EDC) (Sigma-Aldrich, St. Louis, MO, USA) and 1.25 ml of 1M N-hydroxy-succinimide (NHS) (Sigma-Aldrich, St. Louis, MO, USA) [23–27]. After 20 min, the reaction mixture was added to 20 µl of FITC labeled anti-ICAM-1 antibody or PE labeled anti-E-selectin antibody. The EDC/NHS mixture forms an active ester intermediate with GNRs which undergoes amidation reaction with the -NH2 group in the FITC labeled anti-ICAM-1 and PE labeled anti-E-selectin antibodies to yield the conjugate. The reaction mixture was incubated overnight and then the unconjugated antibody was removed. Un-stimulated or stimulated HUVECs were incubated with GNRs conjugated to FITC labeled anti-ICAM-1 or

#141286 - $15.00 USD Received 18 Jan 2011; revised 16 Feb 2011; accepted 17 Feb 2011; published 23 Feb 2011

PE labeled anti-E-selectin on the surface of gelatin coated slide's wells. Additional wells were incubated with GNRs alone with no antibody conjugation (blank GNRs) or with fluorescence dye labeled anti-IgG conjugated GNRs. These wells serve as controls to estimate nonspecific binding levels of GNRs to cells. The concentration of the applied GNRs solution was $10^{12}$ particles/ml ($10^3$ particles/pl) prior to the conjugation process for every case. The gelatin coated slide was then placed in the sample holder of the PA scanning setup depicted in Fig. 2. It should be noted that this concentration is well above the minimum detectable concentration of GNRs of ~$10^{10}$ particles/ml measured in a very thin (less than 1 mm) gelatin phantom under the same experimental conditions as cell experiments, at identical laser fluence (4 mJ/cm$^2$).

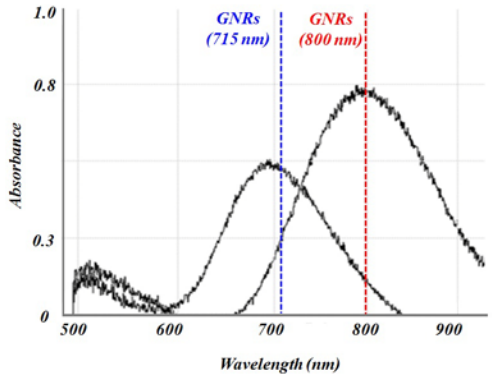


Fig. 1. Optical absorption spectrum of GNRs with aspect ratio of 1:3 (715 nm) and 1:3.5 (800 nm)

### *2.4. Photoacoustic molecular imaging (PMI)*

Figure 2 illustrates the experimental setup for photoacoustic molecular imaging. Nd:Yag pulsed Laser (Quantel, Bozeman, MT, USA) pumps an optical parametric oscillator (OPO, Vibrant HE532I, OpoTek, Carlsbad, CA, USA) to generate 5 ns pulses at 10 Hz. The range of wavelength was tuned from 680 nm to 950 nm. The laser beam of OPO output was directed to illuminate on the surface of cells in the well of the gelatin coated slide (approximately 4 mJ/cm$^2$ of fluence for both 715 nm and 800 nm). The slide was held by a sample holder connected to X-Y-Z manual translational stage for positioning. A focused single element ultrasonic transducer (LiNbO3, 60 MHz, f / 1.5) was used to detect the PA signal. A motorized X-Y translational stage was used to move the transducer to scan horizontally the samples. The typical scan area was about 200 μm by 200 μm and the step size was 10-30 μm, which is about half of the horizontal beam diameter of the ultrasonic transducer. The PA signal was averaged three times at each scanning grid point to minimize the pulse-to-pulse energy variation. The ultrasonic transducer output was amplified (model 5900PR, Olympus, MA, USA), digitized, and recorded by a digital oscilloscope (WaveSurfer 452, LeCroy Corp., NY, USA) synchronized to the laser. The boundary along the circumference and center of each individual well (2 mm in diameter) was identified by eye and used as a global marker to guide for both fluorescence and PA scanning area. Three sets of PA images were obtained at three different locations within this microscopy imaging area of 1000 μm by 700 μm. For PA imaging of multiple targets, the laser light was illuminated at different wavelengths, 715 nm or 800 nm, on the same samples. The laser light beam size was > 10 mm on the surface of the sample, which was large enough to uniformly illuminate the entire sample in the well.

#141286 - $15.00 USD Received 18 Jan 2011; revised 16 Feb 2011; accepted 17 Feb 2011; published 23 Feb 2011

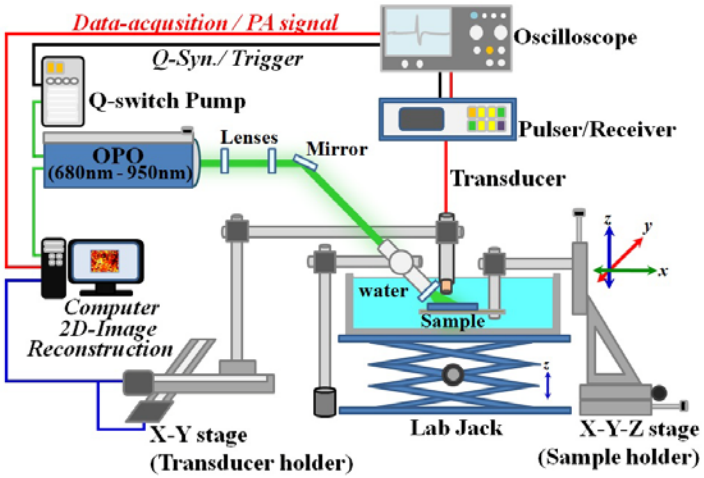


Fig. 2. Experimental set up of photoacoustic molecular imaging. Nd:Yag pulsed Laser, synchronized to the oscilloscope and pulser/receiver, pumps an optical parametric oscillator to generate 5 ns laser pulses at 10 Hz. A focused ultrasonic transducer was used to scan the PA signal over the sample in the water tank.

## 3. Results and discussion

Prior to performing multiple targeting experiments, individual single targeting experiments were performed on each biomarker in a separate set of the experiments. The PA intensity from the stimulated HUVECs was on the average about 8-10 dB higher than the PA intensity from the un-stimulated cells for both ICAM-1 and E-selectin. Control experiments using anti-IgG conjugated GNRs or blank GNRs on both stimulated and un-stimulated HUVECs confirmed low levels of nonspecific binding as measured by PA imaging. PA results in these single targeting experiments compare well with fluorescence imaging results and are consistent with our previous studies under the similar protocols [17,18,28].

With the confirmation of the single targeting of each biomarker, multiple-targeting experiments were performed. FITC labeled anti-ICAM-1 bound GNRs and PE labeled anti-E-selectin bound GNRs solution were mixed, and applied to the stimulated HUVECs. PA intensity images and corresponding fluorescence images from the simultaneous targeting of ICAM-1 and E-selectin on the surface of HUVECs are presented next to each other in Fig. 3. The size of the microscopy image is about 700 μm by 1000 μm. PMI were obtained scanning over an area of 200 μm by 200 μm in 10 μm step increments within the microscopy imaging area. Three sets of PA images were obtained at different locations within the imaging area with similar results. In Fig. 3, the small box in fluorescence image represents the area where PA image was believed to be taken around the center of the well and the large box presents the maximum possible area of misregistration. In Fig. 3, the left panels present bright field ((a) common for both ICAM-1 and E-seletin), fluorescence ((b) ICAM-1, (c) E-selectin) and PA images ((d) ICAM-1, (e) E-selectin) in stimulated conditions. The right panels present bright field ((f) common for both ICAM-1 and E-seletin), fluorescence ((g) ICAM-1, (h) E-selectin) and PA images ((i) ICAM-1, (j) E-selectin) in un-stimulated conditions. Note that all the images of stimulated and un-stimulated cells were obtained from the same batch of the cells. Changing the light filter enables visualization of the FITC labeled ICAM-1 anti-body as well as the PE labeled E-selectin anti-body, and allows for detection of ICAM-1 and E-selectin in the same sample. Subsequently the sample slide was positioned in the sample holder for PA imaging (See Fig. 2) and by changing wavelengths PA images for ICAM-1 at 715 nm and E-selectin at 800 nm were obtained. Overall, PA signal intensity from the stimulated cells displayed increased expression of ICAM-1 (Fig. 3 (d)) and E-selectin (Fig. 3 (e)) compared to that from the un-stimulated cells (Fig. 3 (i), (j)). Increased expression of

#141286 - $15.00 USD Received 18 Jan 2011; revised 16 Feb 2011; accepted 17 Feb 2011; published 23 Feb 2011

ICAM-1 and E-selectin from the stimulated cells compares well with the brightness of fluorescence images (Fig. 3 (b) and (c) respectively). Note a standard linear interpolation was applied to PA raw data in pixels for better presentation.

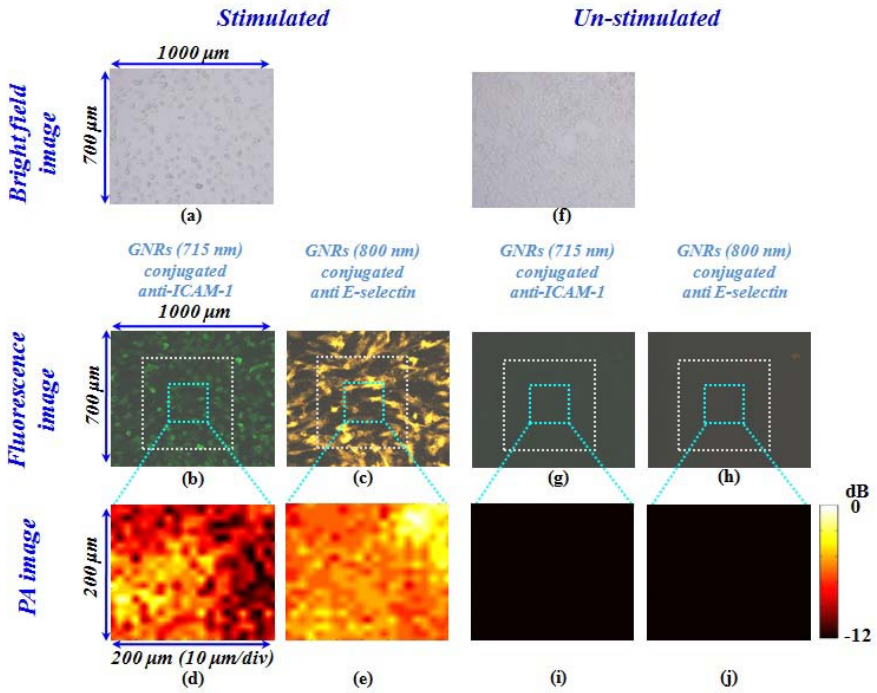


Fig. 3. Simultaneous photoacoustic molecular imaging of the multiple targeted biomarkers of ICAM-1 and E-selectin. The left panels present bright field ((a) common for both ICAM-1 and E-seletin), fluorescence ((b) ICAM-1, (c) E-selectin) and PA images ((d) ICAM-1, (e) E-selectin) in stimulated conditions. The right panels present bright field ((f) common for both ICAM-1 and E-seletin), fluorescence ((g) ICAM-1, (h) E-selectin) and PA images ((i) ICAM-1, (j) E-selectin) in un-stimulated conditions. The small box in fluorescence image represents the area where PA image was believed to be taken around the center of the well and the large box presents the maximum possible area of misregistration. Note the image sizes are not scaled.

In Fig. 4, PA intensity images along with fluorescence images for control groups are presented. The left panels ((a)-(e)) present results for control group in stimulated condition and the right panels ((f)-(j)) present results for control group in un-stimulated condition. Note the bright field images ((a) stimulated, (f) un-stimulated) are common for both IgG of ICAM-1 and E-selectin. As a control, GNRs conjugated to either FITC or PE labeled IgG were exposed to stimulated cells ((b), (c)) and un-stimulated cells ((g), (h)) in the fluorescence images. Corresponding PA images are presented for stimulated cells ((d), (e)) and un-stimulated cells ((i), (j)). As an additional control, blank GNRs were also exposed to stimulated and un-stimulated cells (images not shown). The insignificant PA intensities and low brightness of the corresponding fluorescence images in all these controls compared to signal generated by ICAM-1 or E-selectin conjugated GNRs in stimulated HUVECs (Fig. 3) confirms low levels of nonspecific binding.

#141286 - $15.00 USD Received 18 Jan 2011; revised 16 Feb 2011; accepted 17 Feb 2011; published 23 Feb 2011

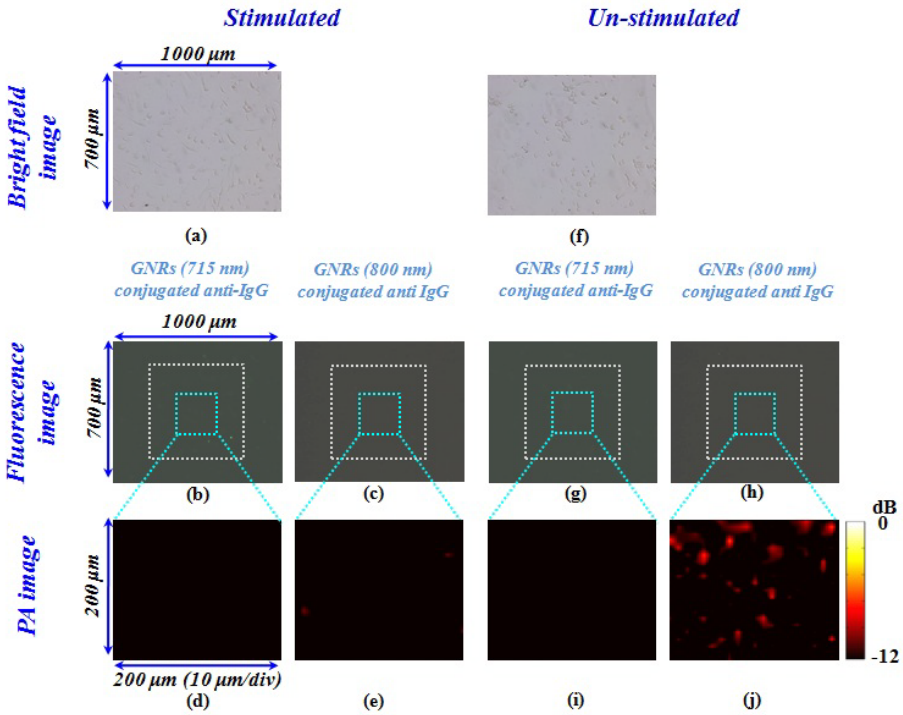


Fig. 4. Simultaneous photoacoustic molecular imaging of the multiple targeted biomarkers of ICAM-1 and E-selectin for control group. The left panels present bright field ((a) common for both anti-IgG of ICAM-1 and E-seletin), fluorescence ((b) anti-IgG for ICAM-1, (c) anti-IgG for E-seletin) and PA images ((d) anti-IgG for ICAM-1, (e) anti-IgG for E-selectin) in stimulated conditions. The right panels present bright field ((f) common for both anti-IgG of ICAM-1 and E-seletin), fluorescence ((g) anti-IgG for ICAM-1, (h) anti-IgG for E-seletin) and PA images ((i) anti-IgG for ICAM-1, (j) anti-IgG for E-seletin) in un-stimulated conditions. The small box in fluorescence image represents the area where PA image was believed to be taken around the center of the well and the large box presents the maximum possible area of misregistration. Note the image sizes are not scaled.

The PA intensities depicted in Fig. 3 and 4 are presented in Fig. 5 as average intensity +/– standard deviation. Each the PA intensity was averaged over the scanning area of 200 μm by 200 μm and presented in dB normalized to PA intensity due to exposure of ICAM-1 targeted GNRs (Fig. 3 (d)) or E-selectin targeted GNRs (Fig. 3 (e)) to stimulated cells. All images were obtained from the same batch of the cells and the cell confluence on each well maintained similar in the order of $3 \times 10^4$ cells/well. Three independent sets of the experiments were performed in each case. In Fig. 5, the blue bar in (a) represents PA intensity due to exposure of ICAM-1 targeted GNRs to stimulated cells. The red bar in (b) represents PA intensity due to exposure of E-selectin targeted GNRs to stimulated cells. The black bars are for PA intensity due to exposure of ICAM-1 or E-selectin targeted GNRs to un-stimulated cells. Green bars represent PA intensity due to exposure of control group, including IgG-conjugated GNRs and blank GNRs added to stimulated and un-stimulated cells and cells only. On the average, PA intensity from the stimulated cells was about 3 folds (~10 dB) higher than that from un-stimulated cells for both ICAM-1 and E-selectin upregulations. Overall, PA intensity from the control groups was minimal and comparable to that from ICAM-1or E-selectin targeted GNRs to un-stimulated cells.

#141286 - $15.00 USD Received 18 Jan 2011; revised 16 Feb 2011; accepted 17 Feb 2011; published 23 Feb 2011

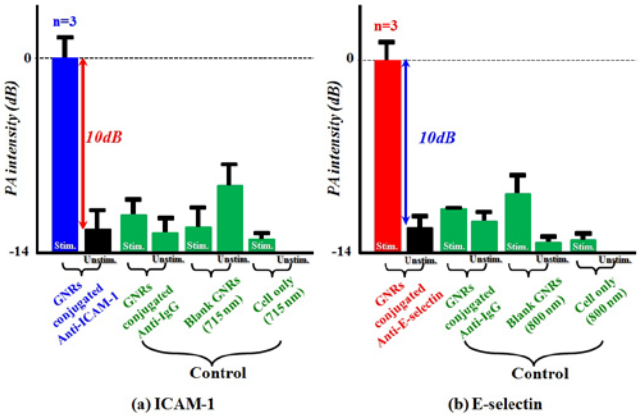


Fig. 5. Average PA intensity of the multiple targeted biomarkers of (a) ICAM-1 and (b) E-selectin. Blue bar: PA intensity due to exposure of ICAM-1 targeted GNRs to stimulated cells. Red bar: PA intensity due to exposure of E-selectin targeted GNRs to stimulated cells. Black bars: PA intensity due to exposure of ICAM-1or E-selectin targeted GNRs to un-stimulated cells. Green bars: PA intensity due to exposure of control group, including IgG-conjugated GNRs and blank GNRs added to stimulated and un-stimulated cells and cells only. Standard deviation for each group of n = 3 is on top of each scale bar.

Figure 6 depicts the fluorescence and PA intensity imaging of single targeted biomarker of ICAM-1 over time. The upper panels ((a)-(d)) present fluorescence images and the lower panels ((e)-(h)) present the corresponding PA intensities at 0, 2, 6, and 24 hours post stimulation. Note a standard linear interpolation was applied to PA data in pixels for better presentation. It is observed that the overall PA signal intensity level monotonically increases as a function of time. The upregulation of ICAM-1 degree at each time point evidenced by fluorescence images follow well the corresponding PA intensity changes.

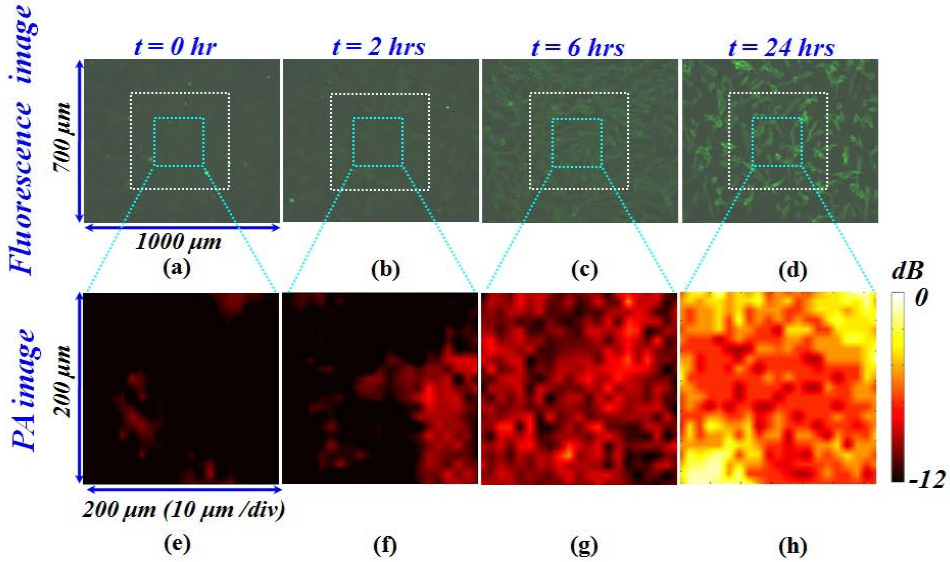


Fig. 6. Time course monitoring of single targeted biomarker of ICAM-1 using fluorescence ((a)-(d)) and photoacoustic molecular imaging ((e)-(h)) at 0, 2, 6, and 24 hours post stimulation. The small box in fluorescence image represents the area where PA image was believed to be taken around the center of the well and the large box presents the maximum possible area of misregistration. Note the image sizes are not scaled.

#141286 - $15.00 USD Received 18 Jan 2011; revised 16 Feb 2011; accepted 17 Feb 2011; published 23 Feb 2011

Figure 7 presents the fluorescence image and PA imaging of single targeted biomarker of E-selectin over time. The upper panels ((a)-(d)) present fluorescence images and the lower panels ((e)-(h)) present the corresponding PA intensities at 0, 2, 6, and 24 hours post stimulation. Compared to ICAM-1, it is observed that the overall PA signal intensity level increases and reaches to the peak earlier at t = 6 hours and decreases thereafter as a function of time. The upregulation of E-selectin degree at each time point evidenced by fluorescence images follow well the corresponding PA intensity changes.

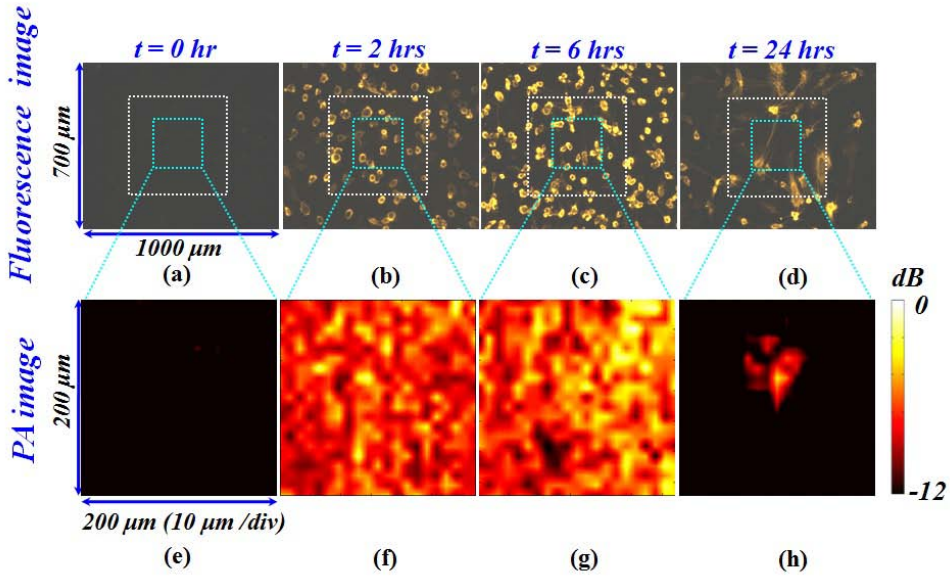


Fig. 7. Time course monitoring of single targeted biomarker of E-selectin using fluorescence ((a)-(d)) and photoacoustic molecular imaging ((e)-(h)) at 0, 2, 6, and 24 hours post stimulation. The small box in fluorescence image represents the area where PA image was believed to be taken around the center of the well and the large box presents the maximum possible area of misregistration. Note the image sizes are not scaled.

With the successful monitoring of the single targeting of each biomarker, time course monitoring of inflammation markers performed using multi-targeting. Figure 8 represents the resulting PA images and fluorescence images of the simultaneous monitoring of ICAM-1 and E-selectin. In Fig. 8, the 1st and 3rd columns present fluorescence images monitoring ICAM-1 and E-selectin respectively, and the 2nd and 4th columns present PA images monitoring ICAM-1 and E-selectin respectively. Alternate fluorescence images were obtained for each sample by simply changing optical filters and alternate PA images were obtained by changing the laser wavelength. Each row in Fig. 8 illustrates the fluorescence and corresponding PA at a specific time point after inflammation was stimulated. The first row represents cells upon stimulation (t = 0), and rows 2, 3 and 4 contain images from cells stimulated for 2, 6, and 24 hours respectively. Overall PA signal intensity level changes compare well the brightness changes, reflecting the degree of the upregulation of each biomarker, in fluorescence image as a function of time (t = 0, 2, 6 and 24 hours post stimulations).

#141286 - $15.00 USD Received 18 Jan 2011; revised 16 Feb 2011; accepted 17 Feb 2011; published 23 Feb 2011

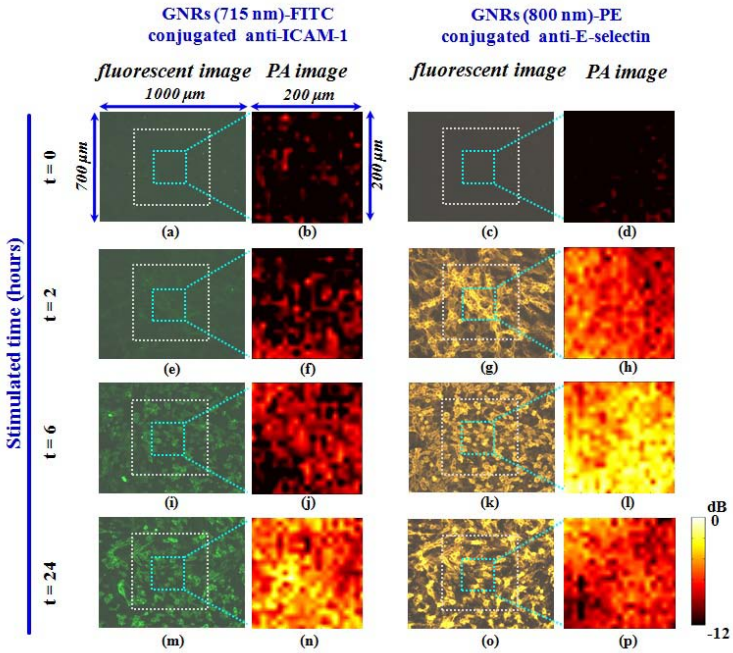


Fig. 8. Time course monitoring of multiple targeted biomarkers, ICAM-1 and E-selectin using photoacoustic molecular imaging. The left two panels present fluorescence (at t = (a) 0, (e) 2, (i) 6, (m) 24 hours) and corresponding PA images (t = (b) 0, (f) 2, (j) 6, (n) 24 hrs) for GNRs (715 nm) conjugated anti ICAM-1 and the right two panels present fluorescence (at t = (c)0, (g)2, (k)6, (o)24 hrs) and corresponding PA images (at t = (d) 0, (h) 2, (l) 6, (p) 24 hours) for GNRs (800 nm) conjugated anti E-selectin at each time point post stimulation. The small box in fluorescence image represents the area where PA image was believed to be taken around the center of the well and the large box presents the maximum possible area of misregistration. Note the image sizes are not scaled.

The PA intensities depicted in Fig. 8 are presented in Fig. 9 as average intensity +/– standard deviation. Three independent sets of the experiments were performed in each case. The blue bars (a) represents PA intensity (dB) +/– standard deviation due to exposure of ICAM-1 targeted GNRs to the stimulated cells at 0, 2, 6 and 24 hours post stimulation. The red bars (b) represent average PA intensity (dB) +/– standard deviation due to exposure of E-selectin targeted GNRs to the stimulated cells at 0, 2, 6 and 24 hours post stimulation.

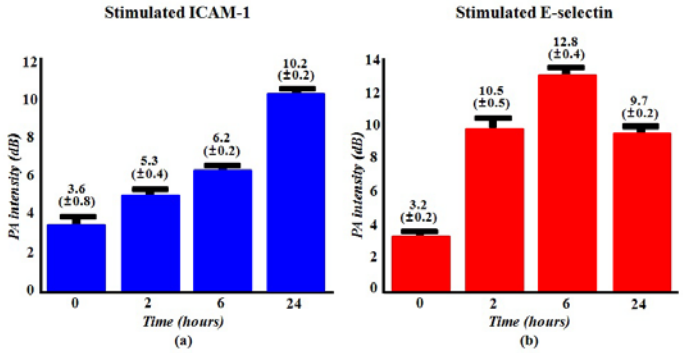


Fig. 9. Average PA intensity at each time point post stimulation for multiple targeted biomarkers of ICAM-1 and E-selectin. Standard deviation for each group of n = 3 is presented on top of each scale bar.

#141286 - $15.00 USD Received 18 Jan 2011; revised 16 Feb 2011; accepted 17 Feb 2011; published 23 Feb 2011

The rt-PCR results of ICAM-1 and E-selectin are plotted in Fig. 10. The scale bars represent the over-expression level of ICAM-1 (a) or E-selectin (b) at each time point of post stimulation. The over-expression of each gene is expressed as fold-over baseline as a function of time +/– standard deviation.

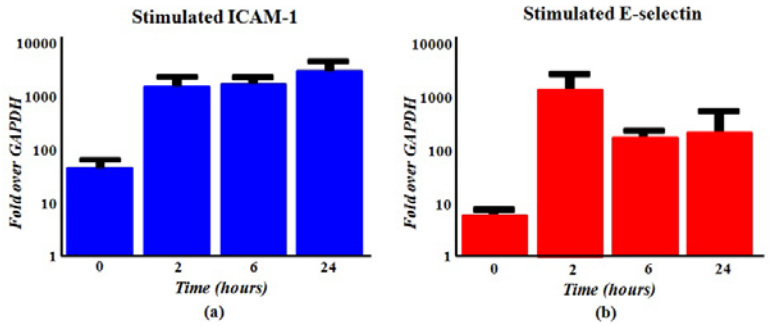


Fig. 10. rt-PCR results of (a) ICAM-1 and (b) E-selectin as function of time (Unit; Fold over baseline)

In summary, the feasibility of the simultaneous detection and monitoring of the multiple inflammatory biomarkers such as ICAM-1 and E-selectin on HUVECs was demonstrated *in vitro*. We have demonstrated that PA signal intensity obtained from ICAM-1 and E-selectin targeted GNRs exposed to cells changes as a function of the time these cells are exposed to inflammatory cytokines, presumably due to increased binding of upregulated cytokines. The upregulation of ICAM-1 and E-selectin in these differentially stimulated cells was confirmed by the immunofluorescence images and rt-PCR. Control experiments using non-specific IgG-conjugated GNRs and blank GNRs added to stimulated and un-stimulated cells confirmed the absence of significant nonspecific binding.

Fluorescence imaging of protein levels as well as rt-PCR to detect and quantify mRNA levels independently demonstrate large degrees of upregulation of ICAM-1 and E-selectin following stimulation. As targeted GNRs are designed to bind to protein, we would hypothesize that the relative levels of inflammatory markers as reported by fluorescence imaging would most accurately predict PA image intensity, and we have found this to be the case in our study. It is important to note that the time course is not identical for both factors, and there are subtle differences between the time course reported by fluorescence imaging and rt-PCR. ICAM-1 expression both at the protein level (detected by fluorescence imaging) and at the mRNA level (detected by rt-PCR) increases over 24 hours. This matches well with data reported in [29]. In the case of E-selectin, mRNA levels peak early on (at 2 hours), and active protein peaks at 6 hours. This roughly agrees with the protein peak reported in [29] of 4 hours, and the mRNA peak reported in [30] of 2-4 hours. It is not surprising to have different temporal peaks in mRNA and protein levels as some time is required to translate mRNA into protein, which must also be transported to the plasma membrane to become available to bind antibody targeted GNRs. We are encouraged to see that the levels of PA intensity match well with protein levels over the complete time course of induction of both ICAM-1 and E-selection, and that these different factors can be monitored simultaneously.

As one of the limitations of the current setup of the experiments, it should be noted that the PMI scanning area was smaller than the fluorescence imaging area due to relatively slow scanning time using a single element transducer. The entire area of the fluorescence image was first scanned coarsely to confirm uniformity of the PMI signal over the region of interest. A smaller PMI area was then chosen with smaller scanning step increments of 10 μm, which is about quarter of the beam width of the transducer in the scanning direction. Another challenge with the current setup of experiments is achieving exact co-registration, in micron scale, between PMI and fluorescence images from two separate systems. With the current

#141286 - $15.00 USD Received 18 Jan 2011; revised 16 Feb 2011; accepted 17 Feb 2011; published 23 Feb 2011

experimental setup, only manual visual co-registration is possible. A photoacoustic molecular imaging setup with confocal capabilities [31,32] would facilitate co-registration in future studies or/and potentially enable individual cell imaging. Although the biocompatibility of GNRs has known to be favorable compared to other nanoparticles [33], to test the potential practical use of this technique, more thorough study on the cell viability along with PA sensitivity using different concentrations of GNRs are required. In this study, the GNRs concentration ($10^{12}$ particles/ml) corresponds to about 10000 particles for a cell of 30 microns (~10 pl). Based on the minimum detectable concentration of GNRs of ~$10^{10}$ particles/ml under laser light fluence of 4 mJ/cm$^2$, about 100 particles per cell can be detected using the current system. A recent development of silica coated GNRs might help with improved stabilization of the particles and augmented PA sensitivity, reducing the required GNRs dose [34].

For the potential PMI applications in vascular diseases *in vivo*, light absorption by blood can be a potential problem if the light source is distant from the object to be imaged. This limitation might be partially circumvented by the use of an optical fiber light delivery system [35], which in conjunction with conventional intravascular ultrasound can access major arteries in deep tissues, such as the coronary tree. Early detection of inflammation could lead to prompt identification and monitoring of many different diseases. In combination with a commercial ultrasound platform, PMI using GNRs as contrast agents may detect inflammatory response at very early stages *in vivo* and potentially monitor the progress of inflammation.

## 4. Conclusion

In conclusion, understanding that the upregulation of leukocyte adhesion molecules is associated with the process of inflammation and plays a major role in thrombus formation and coronary ischemia, specific detection of these biomarkers using bioconjugated gold nanorods (GNRs) could enable monitoring of inflammation using the photoacoustic molecular imaging (PMI) technique. PMI may be able to detect and monitor endothelial upregulation of inflammatory biomarkers *in vivo*.

## Acknowledgments

The work was supported by National Center for Research Resources (NCRR) contract NIH R21HL093176, a component of the National Institutes of Health (NIH) and NIH Roadmap for Medical Research, and its contents are solely the responsibility of the authors and do not necessarily represent the official view of NCRR or NIH. The work was also partially supported by AFOSR MURI 444286-P061716 (N. A. Kotov) and NIH 1R21CA121841-01A2 (N. A. Kotov). The authors thank the University of Michigan's EMAL for its assistance with electron microscopy, and for the NSF grant DMR-9871177 for funding for the JEOL 2010F analytical electron microscope used in this work.

#141286 - $15.00 USD Received 18 Jan 2011; revised 16 Feb 2011; accepted 17 Feb 2011; published 23 Feb 2011